Applied Catalysis B: Environmental 125 (2012) 473–485

Contents lists available at SciVerse ScienceDirect

Applied Catalysis B: Environmental

journal homepage: www.elsevier.com/locate/apcatb

Comparison of the morphology and HDS activity of ternary Ni(Co)-Mo-W catalysts supported on Al-HMS and Al-SBA-16 substrates

R. Huirache-Acuña [a,*], B. Pawelec [b,**], C.V. Loricera [b], E.M. Rivera-Muñoz [c], R. Nava [d], B. Torres [e], J.L.G. Fierro [b]

[a] Facultad de Ingeniería Química, Universidad Michoacana de San Nicolás de Hidalgo, Ciudad Universitaria, 58060, Morelia, Michoacán, Mexico
[b] Instituto de Catálisis y Petroleoquímica, CSIC, c/Marie Curie, 2, Cantoblanco, 28049 Madrid, Spain
[c] Centro de Física Aplicada y Tecnología Avanzada, Universidad Nacional Autónoma de México, A.P. 1-1010, 76000 Querétaro, Mexico
[d] Facultad de Ingeniería, Universidad Autónoma de Querétaro, Centro Universitario, Cerro de las Campanas, 76010 Querétaro, Mexico
[e] University of Texas at El Paso, Materials Research Technology Institute, El Paso, TX, 79968, USA

ARTICLE INFO

Article history:
Received 12 March 2012
Received in revised form 18 May 2012
Accepted 24 May 2012
Available online 1 June 2012

Keywords:
Hydrodesulphurization
Mesoporous systems
Al-HMS
Al-SBA-16
CoMoW
NiMoW catalysts

ABSTRACT

This research compares the hydrodesulphurization (HDS) activity of supported Co(Ni)-Mo-W ternary catalysts with respect to the nature of the support (hexagonal mesoporous silica (HMS) versus SBA-16 material having cage-like mesoporous structure), the type of promoter (Co vs. Ni) and the nature of Al species formed after support modification with Al. Both Al-HMS and Al-SBA-16 mesoporous silica substrates were prepared by the one-pot sol–gel synthesis method via the neutral templating pathway using dodecylamine and Pluronic F127 as surfactants, respectively. The oxide precursors were characterized by a variety of techniques (N_2 adsorption–desorption isotherms, XRD, DRS UV–vis spectroscopy and ^{27}Al NMR), whereas sulphided catalysts were characterized by XPS and HRTEM, and tested in the HDS of DBT conducted in a high-pressure batch reactor at $T = 350\,^{\circ}C$ and $P = 3.1$ MPa. The activity results revealed that NiMoW/Al-HMS catalyst was more active than all Co-promoted catalysts (including a commercial $CoMo/Al_2O_3$ catalyst). The HDS activity was found to be markedly influenced by the textural properties of support and the dispersion of the active phases on the catalyst surface. It has been hypothesised that the presence of extraframework $AlNO_3$ phases on the surface of CoMoW/Al-SBA16 compromises its HDS activity because of the formation of a less active "onion-type" $Mo(W)S_2$ structure.

1. Introduction

Traditionally, sulphur has been removed from petroleum-derived feedstocks by a hydrodesulphurization (HDS) process using alumina-supported Mo or W catalysts promoted by Co or Ni [1,2]. However, to satisfy new stringent environmental restrictions on the sulphur content of fuels, industry is calling for more active HDS catalysts. The new generations of catalysts, such as NEBULA®, are based on a totally different concept of bulk-like materials [3]. In this sense, research on unsupported NiMoW ternary systems has shown that those catalysts record an HDS activity fourfold greater than that of the supported NiMo and NiW catalysts commercially available today [4]. Because the surface properties of bulk catalysts can be easily tuned by supporting them on different substrates, which allows the modification of the dispersion and coordination of the deposited active ingredient, the challenge is to develop supported ternary systems, which could be more active than bulk-like systems.

Current strategies for the design of novel HDS catalysts often include variations in the support formulation, catalyst preparation method and active phase formulation. Regarding research into new supports, a family of highly ordered mesoporous molecular sieves (MMS) has recently attracted the interest of the research community because of their large pores (2–50 nm) and high surface area which allows higher activity per unit weight [5–30]. Among them, the HMS substrate has received particular attention [21–25] because of its interesting wormhole-like or sponge-like framework structure with 2D hexagonal (P6 mm) arrangement of mesopores and channel's branching favouring access to active sites on the framework walls [29]. Since purely siliceous materials have no Brønsted acidity, the isomorphous substitution of Si^{4+} by trivalent cations such as Al^{3+} is of interest because they generate acidity, and these modified supports can be used for acid-catalyzed reactions, such as isomerisation, cracking, hydrotreating and/or alkylation [11–13]. This isomorphous substitution could be performed by the direct mixed-gel synthesis [14] or post-synthesis modifications

* Corresponding author. Tel.: +52 4433167176.
** Corresponding author. Tel.: +34 915 854 769.
E-mail addresses: rafael_huirache@yahoo.it (R. Huirache-Acuña), bgarcia@icp.csic.es (B. Pawelec).

0926-3373/$ – see front matter © 2012 Elsevier B.V. All rights reserved.
http://dx.doi.org/10.1016/j.apcatb.2012.05.034

[15–21], with the latter being used more frequently than the former.

All research into the use of mesoporous silicas modified with Al as supports focuses on the monometallic [4,26] or bimetallic hydrotreating catalysts [3,21,22,24,27]. Concerning the HDS reaction, the results on monometallic MoS_2/Al-HMS catalysts indicated that the HMS mesoporous structure has a unique ability to produce higher activity in the supported MoS_2 phase through metal-support interaction [22]. Interestingly, a comparison of the HDS activities of MoS_2/Al-HMS [22] and WS_2/Al-HMS [23] catalysts with γ-Al_2O_3-supported ones indicated that the Al-HMS-based catalysts record outstanding activity. This was confirmed for Al-HMS-supported Ni- and Co-promoted Mo sulphide catalysts [21]. Klimova et al. [26] studied the effect of the Si/Al ratio on the catalytic response of sulphided NiMo/Al-SBA-15 systems in the HDS of 4,6-DMDBT. It was found that catalytic activity increases with the incorporation of aluminium in the SBA-15 support, peaking at a Si/Al ratio of 20. This increase in activity was linked to the enhancement of the dispersion of oxidic and sulphided Mo species due to the strong interaction of Ni and Mo species with aluminium atoms, which serve as anchoring sites on the support surface [26]. Similarly, it was found that the incorporation of aluminium to the SBA-15 substrate improves the acidic properties of the sulphide Cr/Al-SBA-15 catalysts, providing a stronger metal-support interaction and leading to a better dispersion of chromium species [27].

Contrary to HMS, the SBA-16 substrate has a three-dimensional channel system corresponding to *Im*3*m* space group symmetry and uniform-size pores of a super large cage-like structure with a cubic symmetry [8,9]. In spite of its interesting cage-like structure, the effect of modifying SBA-16 with Al^{3+} ions on the HDS activity of sulphided catalysts has not been widely studied [28], probably because of the difficult synthesis of this substrate [29]. The unique work by Klimova et al. [28] has shown that NiMo catalysts supported on Al-SBA-16, prepared by the post-synthesis alumination of SBA-16, record high activity in the HDS of 4,6-DMDBT. The authors attribute this to the good dispersion of Ni and Mo phases and to the bifunctional character of the catalysts.

In this study, the catalytic performance of the sulphided Ni(Co)MoW catalysts is investigated with respect to the effects of support morphology (Al-HMS vs. Al-SBA-16) and promoter (Co vs. Ni). To best our knowledge, there are no references in the literature to the use of Al-HMS and Al-SBA-16 substrates for supporting trimetallic catalysts, only the effect of promoter was investigated for unsupported Ni(Co)MoW catalysts [30]. The sulphided ternary catalysts have been tested in the HDS of DBT performed in a batch reactor at 350 °C and total pressure of 3.1 MPa. DBT was selected as a model molecule, as this is a typical sulphur-containing compound present in the petroleum fraction of high-boiling point or coal derived liquids.

2. Experimental

2.1. Synthesis of the supports

The Al-HMS (Si/Al atomic ratio of 40) was synthesized following a procedure similar to Zhang et al. [31], via a neutral templating pathway using dodecylamine as the surfactant. In a typical synthesis of Al-HMS substrate, 0.25 mol of dodecylamine were dissolved in 10 mol of ethanol and 130 mol of deionized water. Subsequently, 1.125 mol of mesitylene were added and the solution was stirred for 20 min. Subsequently, a solution of the required amount of tetraethyl orthosilicate (TEOS, 98%, Aldrich) and aluminium isopropoxide (Si/Al = 40) was added to the surfactant solution, which was stirred at room temperature for 20 h. The solid obtained was then filtered, washed thoroughly with deionized water, dried first in air at room temperature and then at 110 °C for 18 h, and finally calcined at 540 °C for 4 h to remove the organic template.

The Al-SBA16 material (Si/Al atomic ratio of 40) was prepared by direct mixed-gel synthesis. The siliceous Al-SBA-16 mesoporous material was synthesized according to the procedure described by Flodström and Alfredsson [32]. Briefly, Pluronic F127 ($EO_{106}PO_{70}EO_{106}$, BASF) triblock copolymer (used as structure-directing) and the corresponding amount of water and 2 M HCl were mixed under stirring. After this, a solution of the required amount of tetraethyl orthosilicate (TEOS, 98%, Aldrich) and aluminium isopropoxide (Si/Al = 40) was added to the surfactant solution, which was stirred at room temperature for 24 h. The mixture was then transferred into polypropylene bottles and heated at 80 °C for 48 h. The solid residue was filtered, washed and dried first at room temperature and then at 110 °C for 24 h. Finally, the sample was calcined at 550 °C in air for 6 h.

2.2. Catalyst preparation

The Al-HMS and Al-SBA16 supports were loaded with fixed amounts of molybdenum (8.53 wt% as MoO_3), tungsten (13.75 wt% as WO_3) and cobalt/nickel (3.81 wt% as CoO or NiO). The concentrations were calculated to achieve a Mo/W atomic ratio of 0.5 and a Ni(Co)/Mo atomic ratio of 0.3. The catalysts were prepared by simultaneous impregnation via the incipient wetness method with aqueous solutions of heptamolybdate tetrahydrate ($(NH_4)_6Mo_7O_{24}.4H_2O$, Aldrich), ammonium metatungstate ($(NH_4)_6H_2W_{12}O_{40}.xH_2O$, Aldrich) and cobalt nitrate hexahydrate ($Co(NO_3)_2.6H_2O$, Aldrich, 98%) or nickel nitrate hexahydrate ($Ni(NO_3)_2.6H_2O$, Aldrich, 98%). The solids obtained were dried at 85 °C for 16 h and then calcined at 500 °C for 4 h.

2.3. Characterization techniques

2.3.1. N_2 adsorption–desorption isotherms

The textural properties of the oxide catalyst precursors and bare supports were determined from the adsorption–desorption isotherms of nitrogen at −196 °C, recorded with a Micromeritics TriStar 3000 apparatus. Prior to the experiments, the samples were degassed at 270 °C under vacuum for 5 h. The volume of the adsorbed N_2 was normalized to standard temperature and pressure. The specific areas of the samples were calculated by applying the BET method to the nitrogen adsorption data within the 0.05–0.25 P/P_0 range. In order to avoid the tensile strength artefact, the pore size distribution (PSD) curves were calculated by applying the Barret–Joyner–Halenda method (BJH) to the adsorption branches of the N_2 isotherms. Total pore volume (V_t) was obtained from the isotherms at $P/P_0 = 0.99$. The micropore volume was estimated using the *t*-plot method. The normalized S_{BET} (NS_{BET}) was calculated from the equation:

$$NS_{BET} = \frac{S_{BET}\ \text{of catalyst}}{[(1-y) \times S_{BET}\ \text{of support}]} \quad (1)$$

where y is the nominal metals content (wt%).

2.3.2. X-ray diffraction (XRD)

The bare supports and oxide catalyst precursors were characterized by powder X-ray diffractometry according to the step-scanning procedure (step size 0.02°; 0.5 s) with a computerized Seifert 3000 diffractometer, using Ni-filtered CuKα ($\lambda = 0.15406$ nm) radiation and a PW 2200 Bragg-Brentano $\theta/2\theta$ goniometer equipped with a bent graphite monochromator and an automatic slit. The assignment of the various crystalline phases was based on JPDS powder diffraction file cards.

2.3.3. DRS UV–vis

The UV–vis diffuse reflectance spectra of the oxide catalyst precursors were recorded in the 200–700 nm range at room temperature using a Varian Cary 5000 UV–vis spectrometer equipped with an integration sphere.

2.3.4. Temperature programmed reduction and desorption (TPR/TPD)

The reduction behaviour of the oxide catalyst precursors was studied by TPR using a Micromeritics TPR/TPD 2900 instrument provided with a thermo conductivity detector (TCD) and interfaced to a data station. The catalyst (0.05 g) was placed on a porous disc inside a 6.3 mm ID U-shaped quartz tube. Prior to reduction, the catalysts (ca. 50 mg) were heated at a rate of 15 °C/min to a final temperature of 250 °C, and kept for 0.5 h at this temperature under a He flow to remove water and other contaminants. The catalysts were cooled to ambient temperature in the same He flow, then reduced in flowing gas containing 10 vol% H_2 in Ar at a total flow rate of 50 mL/min, and finally heated at a rate of 15 °C/min to a final temperature of 1100 °C.

The acidity of the oxide catalyst precursors was determined by the TPD of ammonia measurements carried out with the same apparatus described for TPR. After loading, the sample of 0.050 g was pre-treated in a He (Air Liquide, 99.996%) stream at 250 °C for 1 h. Following this, the sample was cooled to 100 °C and ammonia-saturated in a stream of 5% NH_3/He (Air Liquide) flow (50 mL/min) for 1 h. Following catalyst equilibration in a He flow at 100 °C for 15 min, the ammonia was desorbed using a linear heating rate of 15 °C/min to 550 °C. In order to determine the total acidity of the catalyst from its NH_3 desorption profile, the area under the curve was integrated. A semiquantitative comparison of the acid strength distribution was made by Gaussian deconvolution of the peaks.

2.3.5. ^{27}Al nuclear magnetic resonance (^{27}Al NMR)

Solid-state CP MAS ^{27}Al NMR measurements were recorded on a Bruker AV 400 WB spectrometer. The dried oxide catalyst precursors were loaded into a BL_4 X/Y/^{1}H 4-mm multinuclear probe and spun at 5 kHz according to the following protocol: $\pi/2$ pulse, 7 μs; CP contact time 2 ms; 1700 scans. An internal reference on the spectrometer was used to calculate chemical shifts. The samples were dried at 250 °C for 2 h.

2.3.6. High resolution transmission electron microscopy (HRTEM)

HRTEM microscopy studies of fresh sulphided catalysts were carried out using a JEM 2100F microscope operating with a 200 kV accelerating voltage and fitted with an INCA X-sight (Oxford Instruments) energy dispersive X-ray microanalysis (EDX) system to verify the semi-quantitative composition of supported phases. Freshly sulphided catalysts were ultrasonically dispersed in acetone at room temperature and then spread out on a holey carbon–copper microgrid.

2.3.7. X-ray photoelectron spectroscopy (XPS)

The photoelectron spectra of ex situ fresh sulphided catalysts were recorded on a VG Escalab 200R spectrometer equipped with a hemispherical electron analyzer and an Mg Kα ($h\nu$ = 1253.6 eV) X-ray source. The experimental procedure followed during XPS measurements has been described elsewhere [30]. The binding energies (BE) were referenced to the C 1s peak (284.9 eV) to account for charging effects. The areas of the peaks were computed after the fitting of the experimental spectra to Gaussian/Lorentzian curves and the removal of the background (Shirley function). Surface atomic ratios were calculated from the peak area ratios normalized by the corresponding atomic sensitivity factors.

2.4. Catalytic activity measurements

In this work, the HDS of DBT was carried out in a Parr model 4575 high-pressure batch reactor. The particle size of all catalysts studied was in range 0.10–0.15 mm because our previous studies demonstrated that catalyst having particle size below 0.2 mm are free of diffusion effects in the HDS reaction performed in a batch reactor. Prior to the catalytic test, the oxide catalyst precursors were sulphided ex situ at atmospheric pressure in a tubular furnace heated to 400 °C (4 °C/min) under a flow of H_2S in hydrogen (15%) and kept under those conditions for 4 h. The sample was then cooled to room temperature under a N_2 flow. All the catalysts were sulphided by the same procedure. The sulphided catalyst (ca. 0.5 g) was then introduced into the batch reactor containing a solution of 5 vol% of DBT in decalin ($[DBT]_0$ = 0.239 mol/L]. The reactor was then pressurized to 3.1 MPa with hydrogen and heated to 350 °C at a rate of 10 °C/min. The stirring rate of the reaction mixture was sufficiently intense (600 rpm) to exclude external diffusion limitations. Once working temperature had been reached, sampling for chromatographic analysis was performed during each run to determine conversion versus time dependence. The reaction time was averaged to 5 h. The resulting products were analyzed using a Perkin Elmer gas chromatograph provided with a 3-m packed column containing 3% OV-17 as separating phase on a Chromosorb WAW 80/100.

The compounds detected by GC were biphenyl (BP), cyclohexylbenzene (CHB) and traces of tetrahydrodibenzothiophene (THDBT). The total DBT conversion was calculated as DBT disappearance, and direct desulphurization (DDS) and hydrogenation (HYD) selectivity were defined as:

$$\text{DDS}: \frac{(\text{BP}) \times 100\%}{(\text{CHB} + \text{BP} + \text{THDBT})} \quad (2)$$

$$\text{HYD}: \frac{(\text{CHB} + \text{THDBT}) \times 100\%}{(\text{CHB} + \text{BP} + \text{THDBT})} \quad (3)$$

HDS kinetic constants (k) were calculated assuming pseudo-first order kinetics referred to initial DBT concentration [33].

$$kt = -\ln(1 - x) \quad (4)$$

where t is reaction time, and x is the conversion of DBT.

A commercial $CoMo/Al_2O_3$ (Akzo KF-752; Mo = 14.2%; Co = 3.8%; P = 0.83%; S_{BET} = 223 $m^2\,g^{-1}$; average pore diameter = 6.6 nm) provided by Akzo Nobel was used as reference.

3. Results and discussion

3.1. Characterization of oxide precursors

3.1.1. Textural properties

The low-angle X-ray diffraction patterns of naked Al-HMS and Al-SBA16 supports are shown in Fig. 1. As seen in this figure, the Al-HMS substrate has an intense single d_{100} reflection accompanied by more or less pronounced diffuse scattering centred at 1.73°, which indicates hexagonal symmetry. Higher-order Bragg reflections are not resolved in the patterns of this sample. However, similar "single-reflection" materials can still have local hexagonal symmetry, as observed by selected area electron diffraction and TEM [34]. On the other hand, the Al-SBA16 sample has well defined 110, 200 and 211 reflections corresponding to a cubic structure ($Im3m$) of the SBA-16 substrate [8]. Thus, the low-angle XRD demonstrated that both Al-HMS and Al-SBA-16 preserved their structure after calcination at 550 °C.

The textural properties of the bare supports (Al-HMS and Al-SBA16) and oxide precursors were studied by N_2 physisorption at −196 °C (Fig. 2). As expected, a large decrease in the amount of

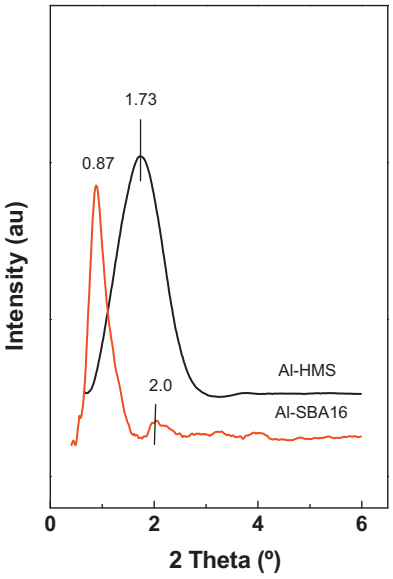

Fig. 1. Small-angle XRD patterns of naked supports.

adsorbed nitrogen is observed after the incorporation of a large amount of metal oxides on both supports. The N_2 isotherms of all samples are of type IV [35]. The shape of the isotherms of both CoMoW/Al-HMS and NiMoW/Al-HMS catalysts are similar to those of the naked Al-HMS material, indicating that the porous characteristics of the support have not been damaged after metal loading followed by calcination. The N_2 isotherms of both Al-HMS-based samples have two capillary condensation steps: (i) the first hysteresis loop for these materials starts at a partial pressure of about 0.40, indicating the presence of framework mesoporosity; and (ii) the second hysteresis loop starting at a relative pressure of about 0.88 might be attributed to either macropores or textural inter-particle mesoporosity, which takes place when the particle diameters are very small and closely packed [36]. On the other hand,

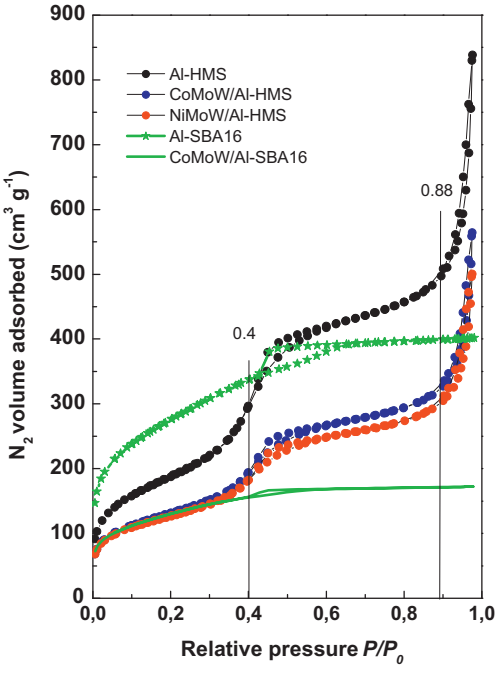

Fig. 2. Nitrogen adsorption–desorption isotherms of naked supports and oxide precursors.

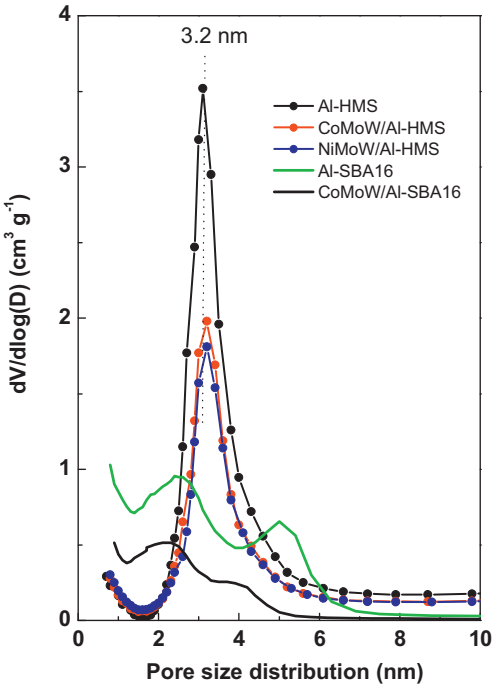

Fig. 3. Pore size distribution of naked supports and oxide precursors as determined from adsorption branch of the N_2 adsorption data using the BJH method.

the CoMoW/Al-SBA16 oxide catalyst precursor records type IV N_2 isotherms with type H1 hysteresis loop [37]. As compared with the pure Al-SBA16 support, the CoMoW/Al-HMS oxide catalyst precursor shows a shift of the inflection point of its hysteresis to lower values of the relative pressures (from 0.40 to 0.38 P/P_0). This shift could be induced by the confinement effect of CoMoW metal oxide particles located inside the inner structure of SBA-16.

Table 1 summarizes the values of specific BET surface areas (S_{BET}), total pore volume (V_{total}) and average pore diameter (d) of the naked supports and oxide precursors. As expected, both S_{BET} and V_{total} decrease after metal oxide incorporation during catalyst preparation. It is noteworthy that, regardless of the support, all oxide precursors have a very similar S_{BET} (within the 448–471 $m^2\,g^{-1}$ range) and a large difference in V_{total}, with both Al-HMS-based catalysts having higher values. Since the NiMoW/Al-HMS oxide catalyst precursor records only a slightly lower S_{BET} than its CoMoW/Al-HMS counterpart (471 vs. 451 $m^2\,g^{-1}$), similar metal oxide dispersion on the support surface could be expected for both catalysts. Considering experimental error values, the CoMoW/Al-HMS sample recorded a similar average pore diameter value (5.0 nm) and pore volume (0.87 $cm^3\,g^{-1}$) to the NiMoW/Al-HMS sample (4.7 nm and 0.77 $cm^3\,g^{-1}$, respectively). Fig. 3 show the pore size distribution of the naked supports and oxide catalyst precursors as determined from adsorption branch of the N_2 adsorption data using the BJH method. The two Al-HMS-supported oxide catalyst precursors show relatively narrow pore size distribution centred at 3.2 nm. On the contrary, the CoMoW/Al-SBA16 sample shows bimodal pore size distribution centered at about 2.5 and 4 nm. Thus, one might expect that this dual-porosity system makes the Al-SBA16 material superior candidate for catalysis application than its Al-HMS counterpart. However, a larger difference of the average pore diameter between CoMoW/Al-HMS and CoMoW/Al-SBA16 (5.0 vs. 1.7 nm) is critical for the final catalytic performance of the respective supported catalysts.

SBA-16 is known to contain micropores within the walls of primary mesopores forming a three-dimensional channel system with connections between the mesopores [8,9]. Thus, the large loss of

Table 1
Textural properties[a] and ^{27}Al NMR data of oxide precursors.

Samples	S_{BET} ($m^2\ g^{-1}$)	NS_{BET}	V_{total} ($cm^3\ g^{-1}$)	d (nm)	^{27}Al signal (ppm)
NiMoW/Al-HMS	451 (689)	0.87	0.77 (1.30)	4.7 (5.0)	51.9 2.9
CoMoW/Al-HMS	471 (689)	0.91	0.87 (1.30)	5.0 (5.0)	55.3 41.0 31.8 5.9 1.7
CoMoW/Al-SBA16	448 (953)	0.64	0.267 (0.62)	1.7 (1.8)	107.6 66.7 58.1

[a] As determined from N_2 adsorption–desorption isotherms at −196 °C. S_{BET}: specific BET surface area; NS_{BET}: normalized S_{BET} calculated using Eq. (1); V_{total}: total pore volume; d: average pore diameter calculated from adsorption data by BJH method. Data of naked supports are given in parenthesis.

V_{total} after metal loading suggests the loss of microporosity, which is probably due to pore blocking by guest metal oxides. To confirm the location of guest phases, the normalized BET surface area (NS_{BET}) was calculated with Eq. (1). The NS_{BET} of oxide catalyst precursors are listed in Table 1. For both Al-HMS-based samples, the NS_{BET} value close to 0.9 suggests the bimodal location of the metal oxides on the external surface and within the inner porous structure (larger fraction). As compared with those samples, the NS_{BET} of the CoMoW/Al-SBA16 sample is relatively low (0.64), indicating some blocking of the support pores by the guest particles.

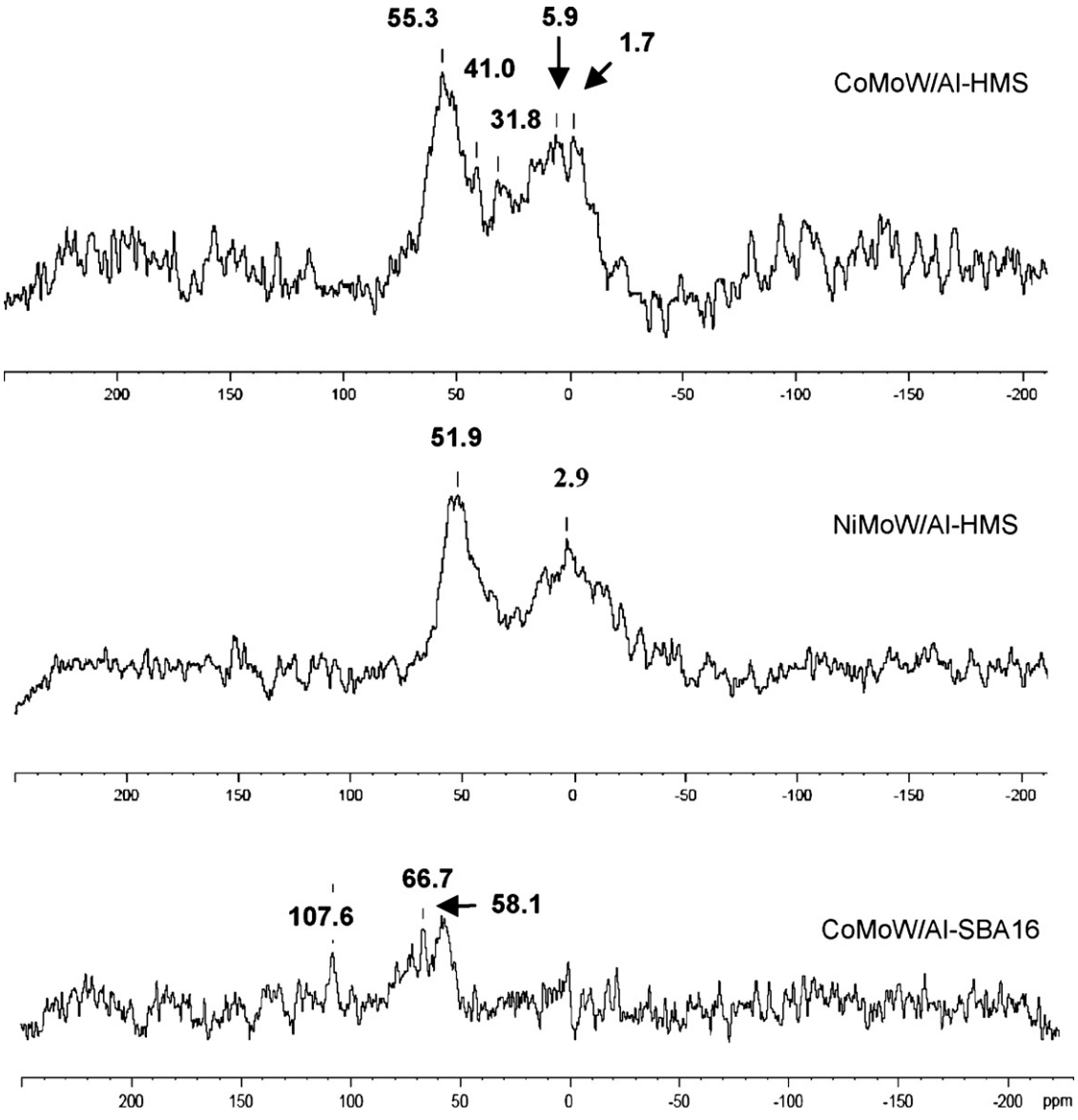

Fig. 4. ^{27}Al NMR profiles of oxide catalyst precursors.

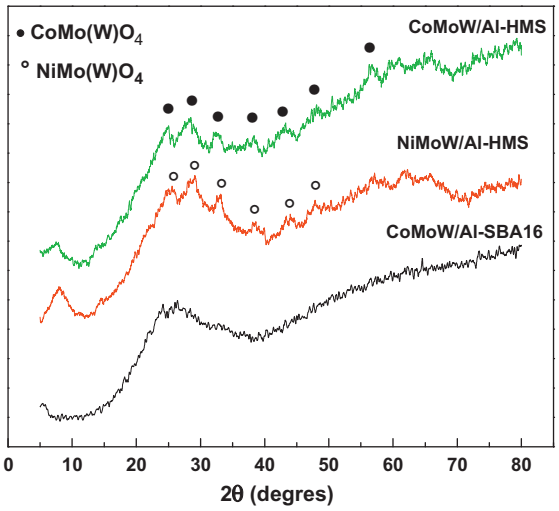

Fig. 5. Wide-angle XRD patterns of oxide precursors.

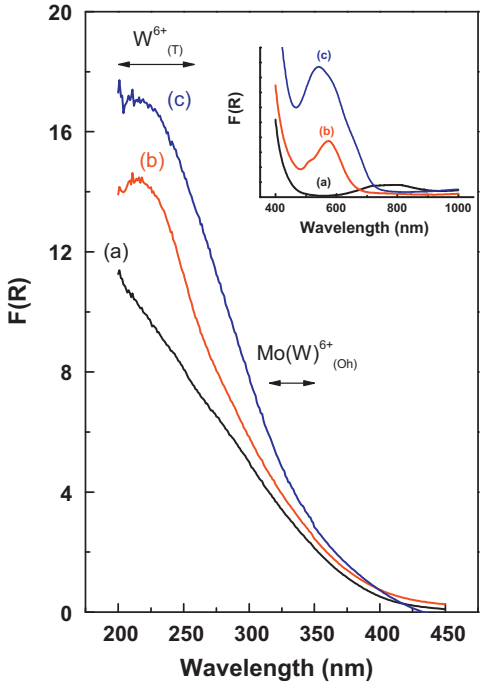

Fig. 6. DRS UV–vis spectra of oxide catalyst precursors: (a), NiMoW/Al-HMS; (b), CoMoW/Al-HMS; and (c), CoMoW/Al-SBA16.

3.1.2. Nuclear magnetic resonance (^{27}Al-NMR)

More detailed information can be obtained from ^{27}Al NMR MAS spectra, which reveal the coordination of Al atoms in the samples under study. Fig. 4 shows the ^{27}Al NMR spectra of all oxide catalyst precursors and Table 1 summarizes their ^{27}Al NMR signal positions. The ^{27}Al NMR spectra of the CoMoW/Al-HMS sample record the signal for tetrahedrally coordinated aluminium at 55.3 ppm and a few small signals at 41.0, 31.8, 5.9 and 1.7 ppm. The signal at 31.8 ppm is probably due to pentacoordinated Al atoms [38], whereas the signals at 5.9 and 1.7 ppm could be due to octahedrally coordinated Al atoms (extraframework Al species) [39]. Besides the use of the same support, the ^{27}Al NMR spectra of the NiMoW/Al-HMS sample reveal certain differences compared to its Co-promoted counterpart. Thus, the ^{27}Al NMR spectra of NiMoW/Al-HMS sample record the presence of two signals due to Al^{3+} ions in two different environments: one peak at about 51.9 ppm and another peak at about 2.9 ppm, in accordance with the literature [40]. The former sharp peak is due to 4-coordinated structural aluminium species, whereas the signal at about 2.9 ppm is due to extraframework Al in octahedral coordination [41]. Consistent with the study by Chiranjeevi et al. [40], our ^{27}Al NMR spectra indicate that a larger amount of Al is incorporated into the framework of the HMS than in extraframework positions. Contrary to both Al-HMS-based catalysts, the CoMoW/Al-SBA16 sample shows peaks at 107.6, 66.7 and 58.1 ppm. The latter two peaks indicate that this sample possesses a large proportion of the Al inserted into tetrahedral positions within the framework of SBA-16. The peak at 107.6 ppm comes likely from $Al(NO_3)_3$ [42].

Summing up, the ^{27}Al NMR spectra measurements of both Ni and Co promoted catalysts evidenced the presence of a significant amount of Al in a tetrahedral environment, indicating the incorporation of Al atoms in the framework structure of the HMS substrate. The presence of octahedral Al species in both Al-HMS-based samples is probably due to the low solubility of the precursor in the synthesis gel and/or partial framework dealumination during the calcination process [41]. For the CoMoW/Al-SBA16 sample, a large amount of the extraframework aluminium species might contribute to its largest pores becoming blocked by guest molecules, as deduced from its lowest normalized specific surface area (Table 1).

3.1.3. Wide-angle X-ray diffraction

Wide-angle XRD profiles were recorded to investigate the presence of any crystallite species in the catalysts. Fig. 5 illustrates the diffraction profiles of Al-HMS- and Al-SBA16-based oxide catalyst precursors. All oxide catalysts reveal typical diffraction patterns, with a very broad peak at around $2\theta = 24^\circ$, typical of amorphous silica [43]. The XRD pattern of the CoMoW/Al-HMS sample records peaks at $2\theta = 25$, 28, 32.5, 38, 43, 48, 57 and 59.5° corresponding to the β-$CoMoO_4$ phase (JCPDS-ICDD 21-868), whereas the peaks corresponding to the $NiMo(W)O_4$ phase (JCPDS-ICDD 33-0948) were observed for the NiMoW/Al-HMS sample. The formation of large β-$Co(Ni)Mo(W)O_4$ crystallites could be linked to the presence of extraframework aluminium oxide species on the surface of both Al-HMS-based samples (vide supra ^{27}Al NMR). By contrast, the XRD pattern of the CoMoW/Al-SBA16 catalyst containing $AlNO_3$ species on its surface did not record the diffraction lines of any crystalline phases (Fig. 5). This points to different interfacial transformations [44,45] that occur upon simultaneous adsorption of $Co(H_2O)_6^{2+}$ aqua complexes and molybdate/tungstate species on both Al-HMS and Al-SBA16 supports.

3.1.4. UV–vis diffuse reflectance spectra (DRS)

The coordination environment of $Ni(Co)^{2+}$ and $Mo^{6+}(W^{6+})$ ions in the calcined catalysts was studied by UV–vis diffuse reflectance spectroscopy. The DRS spectra of the oxide catalysts precursors are plotted in Fig. 6 as a Schuster–Kubelka–Munk function. Regardless of the promoter, all catalysts record two strong bands in ranges 210–270 nm and 320–350 nm. The first one implies the presence of a ligand-to-metal charge transfer involving isolated transition metal sites, which is ascribed in the literature to tungsten in tetrahedral coordination, like that in the WO_4^{2-} group [46], but different from that in the WO_3 crystal [47]. The second one is assigned to the O^{2-}-Mo^{6+} (W^{6+}) ligand-to-metal charge transfer transition (LMCT) of molybdenum or tungsten ions with octahedral coordination [48,49].

Considering the XRD results of the CoMoW/Al-HMS sample, the UV–vis absorption band at about 320 nm could be tentatively ascribed to $CoMo(W)O_4$ phases [50]. However, considering the very close position of the band indicative of polymolybdates (300 nm) [50], the superposition of the absorption bands of cobalt molybdates and polymolybdates-like species cannot be excluded. Considering the intensity of the bands indicative of

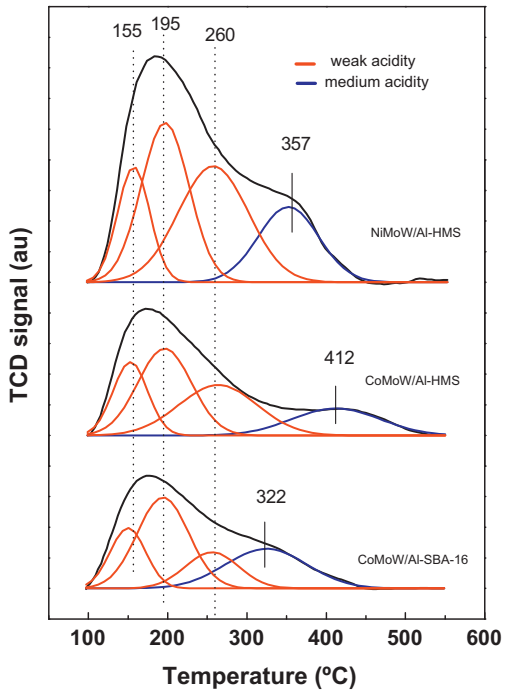

Fig. 7. TPD profiles after NH_3 adsorption at 100 °C on oxide precursors.

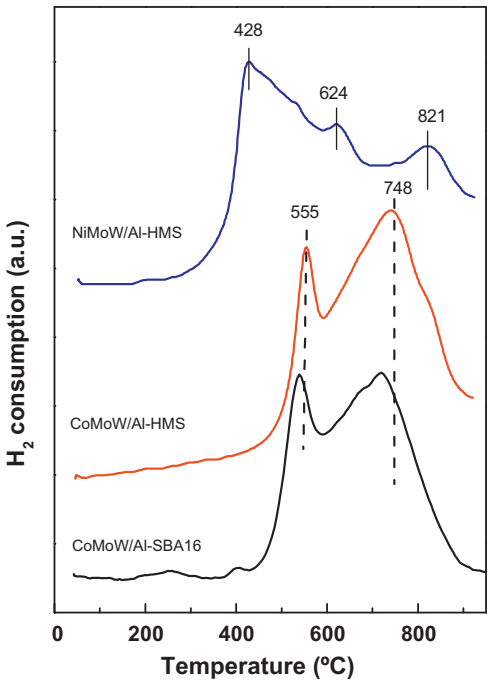

Fig. 8. TPR profiles of oxide precursors.

Mo(W) species in tetrahedral coordination, the observed trend is CoMoW/Al-SBA16 > CoMoW/Al-HMS > NiMoW/Al-HMS. It is noteworthy that both Al-HMS-based catalysts have a very similar amount of Mo^{6+}(W^{6+}) ions in octahedral coordination and a lower amount of those ions than their CoMoW/Al-SBA16 counterpart, indicating that the formation of the species with Mo^{6+}/W^{6+} ions in tetrahedral and octahedral coordination is favoured on the CoMoW/Al-SBA16 sample.

Finally, it should be noted that the CoMoW/Al-SBA16 sample is unique, with a band at about 540 nm (see inlet in Fig. 5), which is ascribed to *d–d* transitions ($^4T_{2g}$ to $^4A_{2g}$ and $^4T_{2g}$ to $^4T_{1g}$ (P)) of high spin octahedral Co complexes [51,52]. A similar band observed at 520 nm was ascribed to Laporte-forbidden but spin-allowed *d-d* transitions of Co(II) ions [53]. Thus, for the CoMoW/Al-SBA16 sample, the formation of undesirable $CoSiO_4$ species could be inferred. For the NiMoW/Al-HMS sample, Ni^{2+} ions were detected in octahedral coordination (band at 750 nm) [54].

3.1.5. Temperature-programmed desorption of NH_3 (TPD-NH_3)

The TPD of ammonia was carried out in order to assess the effect of support's grafting by Al^{3+} ions on the acidity of oxide precursors, without distinguishing between Brønsted and Lewis acid sites. The acidity of the sulfided catalysts was not studied because it is well known that sulfidation led to formation of —SH groups attached to the support surface and this might mask the effect of support grafting. Moreover, there is limitation of the use of probe molecules such as NH_3, pyridine or acetonitrile for the study of acidity of sulfided catalysts by TPD or FTIR/DRIFT techniques. This is because Mo(W)-based sulfides are also hydrodenitrogenation catalysts implying that nitrogen species chemically adsorb on the active sites as well.

The TPD profiles of NH_3 adsorbed at 100 °C on oxide precursors are shown in Fig. 7. All TPD-NH_3 profiles were mathematically analyzed using Gaussian functions. Depending on the temperature ranges in which the ammonia was desorbed, the acid sites distribution pattern was classified into weak (ammonia desorption at $T < 300$ °C) and medium (desorption in the 300–500 °C range). The concentration of different acid sites, expressed as mmol of desorbed NH_3 per g of catalyst, is reported in Table 2. As seen in this table, the observed trend for the weak and total acid sites is as follows: NiMoW/Al-HMS > CoMoW/Al-HMS > CoMoW/Al-SBA16, in good agreement with ^{27}Al NMR (vide supra). Thus, the NiMoW/Al-HMS sample has a larger number of acid sites available to NH_3 chemisorption than both Co-promoted samples.

3.1.6. Temperature-programmed reduction (TPR)

The TPR profiles of the oxide precursors are shown in Fig. 8 whereas H_2 uptake values are listed in Table 2. The TPR profiles of the NiMoW/Al-HMS and CoMoW/Al-HMS samples record a narrow peak at 428 °C and 555 °C, respectively. This narrow peak could be ascribed to the formation of Mo(W) species interacting with Ni/Co, as well as to nickel/cobalt oxide species, which are more easily reduced than $Mo(W)O_3$. For the CoMoW/Al-SBA16 sample, this latter peak is shifted to a lower temperature (555 vs. 537 °C), indicating an easier reduction in the oxide species supported on Al-SBA16 with respect to those supported on Al-HMS. For all catalysts, the large hydrogen consumption in the 500–900 °C region contains probable peaks belonging to the two-step reduction in $Mo(W)O_3$ species interacting strongly with the support [55]. Contrary to NiMoW/Al-HMS, the TPR results suggested strong interactions between Mo(W) and Co on the surface of both the Al-HMS and Al-SBA16 samples.

3.2. Characterization of fresh sulphided catalysts

Since metal sulphides are the active phases in the HDS reaction, the fresh sulphided catalysts were studied by both HRTEM and XPS techniques. Concerning the support morphology, HRTEM images confirmed the regular porous arrangement of the Al-SBA16- and Al-HMS-based sulphide catalysts (not shown here). Thus, the SBA16-based sample has a regular pore structure along [1 0 0] and [1 1 1] directions corresponding to a cubic *Im3m* structure. In addition, some distorted and collapsed areas can be distinguished. As expected, after sulphidation all catalysts display the typical fringes of MoS_2 (WS_2) crystallites. In Fig. 9(a)–(c), high magnification $Mo(W)S_2$ sheets are compared. For all catalysts, the arrangement of $W(Mo)S_2$ layers parallel to the substrate indicates

Table 2
Acidic properties[a] and H_2 uptake[b] of oxide precursors.

Catalyst	Amount of acid sites[a] (mmol NH_3 g_{cat}^{-1})			H_2 uptake[b] (μmol/g_{cat})
	Weak T_{max} < 300 °C	Medium T_{max} = 300–450 °C	Total	
NiMoWS/Al-HMS	1.41	0.33	1.74	1.19
CoMoWS/Al-HMS	0.81	0.17	0.98	1.37
CoMoWS/Al-SBA16	0.64	0.23	0.87	1.37

[a] As determined by TPD-NH_3.
[b] As determined by TPR.

Table 3
HRTEM data of sulphided catalysts.

	NiMoW/Al-HMS	CoMoW/Al-HMS	CoMoW/Al-SBA16
Average length of layers (nm)	5.4 ± 1.8	4.8 ± 1.9	6.5 ± 3.5
Stacking number of layers	4.0 ± 1	4.0 ± 1	4.0 ± 1
Surface density Mo(W)S_2 particles/1000 nm^2	25 ± 6	21 ± 3	22 ± 5

Table 4
Binding energies (eV) of elements in the sulphided catalysts (from XPS).

Catalysts	Si 2p	Mo3$d_{5/2}$	Ni2p or Co2p	W 4$f_{7/2}$	S 2p	Al2p
NiMoWS/Al-HMS	103.4	228.9	854.2	32.1 (74) 35.8 (26)	161.8	74.3
CoMoWS/Al-HMS	103.4	228.9	778.8 (61) 780.6 (39)	32.5 (85) 36.0 (15)	162.0	74.6
CoMoWS/Al-SBA16	103.4	228.9	778.2 (57) 780.6 (43)	32.3 (36) 34.0 (33) 35.5 (31)	161.9	74.6

the basal plane attachment. No edge-plane attachment was observed because such species easily escape detection. The Ni-promoted sample has higher W(Mo)S_2 slab density than the two Co-promoted counterparts (Table 3). The interlayer spacing of all catalysts was similar and a little larger than for the pure Mo(W)S_2 phase (0.71 vs. 0.62 nm). It is noteworthy that contrary to Al-HMS-based samples, the CoMoW/Al-SBA16 catalyst has the disordered curved fringes of the W(Mo)S_2.

More information on the morphology of phases formed can be revealed by the statistical evaluation of around 250 particles from various HRTEM images. Table 3 summarizes the average length and stacking number of the Mo(W)S_2 particles, whereas Fig. 10 shows the statistical analysis of Mo(W)S_2 particle length. TEM data are evaluated as follows: (i) the morphology of the support might influence particle length, since smaller Mo(W)S_2 particles were formed on both Al-HMS-based catalysts than on CoMoW/Al-SBA16; (ii) all catalysts recorded highly stacked layers of Mo(W)S_2 particles (4 ± 1 layers); and (iii) the surface density of Mo(W)S_2 particles follows the trend: NiMoW/Al-HMS > CoMoW/Al-HMS ≈ CoMoW/Al-SBA16.

The chemical state and surface composition of freshly sulphided catalysts were revealed also by XPS. The Ni 2$p_{3/2}$ and Co 2*p* core level spectra are shown in Fig. 11(a) and (b), respectively, whereas the S 2*s* Mo 3d and W 4f core level spectra are shown in Fig. 12(A) and (B), respectively. The binding energies of the most intense photoelectron Si 2p, Mo 3$d_{5/2}$, Ni(Co) 2$p_{3/2}$ and W 4$f_{7/2}$ peaks are compiled in Table 4, while the quantitative XPS analysis data are shown in Table 5. For all catalysts, the Si 2p core level peak was close to 103.4 eV, which is characteristic of SiO_2. Thus, regardless of the support, the chemical environment of silicon ions was not affected by the presence of Al atoms. For all catalysts, the S 2*p* signal was evaluated and the result of the fit was a contribution by the S 2$p_{3/2}$ signal centred at 161.2 ± 0.1 eV, which is characteristic of S^{2-} ions.

For the NiMoW/Al-HMS sample (Fig. 11(A)), the Ni 2$p_{3/2}$ binding energy of 854.2 eV indicated the formation of bulk Ni_2S_3 phase [56,57]. The binding energy of nickel in Ni_2S_3 is slightly higher than that reported for bulk species (854.2 vs 854.1 eV). The same small BE shift was reported previously for unsupported Ni-W sulphide hydrotreating catalysts [58]. The differences of BE allow us to infer that a major fraction of Ni is in the form of "Ni-Mo(W)-S" phase [58]. It was concluded from the Ni 2*p*/S 2*p* intensity ratio that the sulphidation of Ni is complete. This is consistent with TPR results (Fig. 8), indicating that the nickel species of the NiMoW/Al-HMS sample are reduced at a lower temperature than the cobalt species of both Co-promoted counterparts.

For the two Co-promoted catalysts, the Co 2*p* core-level spectra showed two contributions of the Co 2$p_{3/2}$ component (Fig. 11(b)): a minor one at 778.2–778.3 eV indicative of CoS_2 species [57] and another one at 780.9 ± 0.1 eV indicative of Co^{2+} ions surrounded by oxygen atoms [57], as deduced from the low-intensity shake-up satellite observed on the high-binding-energy side. For the two Co-promoted catalysts, the formation of "Co-Mo-S" phase is highly possible because in the literature is largely described that

Table 5
Surface atomic ratios of sulphided catalysts (from XPS).

Catalysts	Ni(Co)/Si at	Mo/Si at	W/Si at	Me/Si at	Al/Si at	S/Si at	S/Me at
NiMoWS/Al-HMS	0.009	0.023	0.019	0.051	0.025	0.071	1.39
CoMoWS/Al-HMS	0.019	0.022	0.021	0.062	0.037	0.071	1.15
CoMoWS/Al-SBA16	0.015	0.013	0.010	0.038	0.030	0.044	1.17

Me: Co(Ni) + Mo + W.

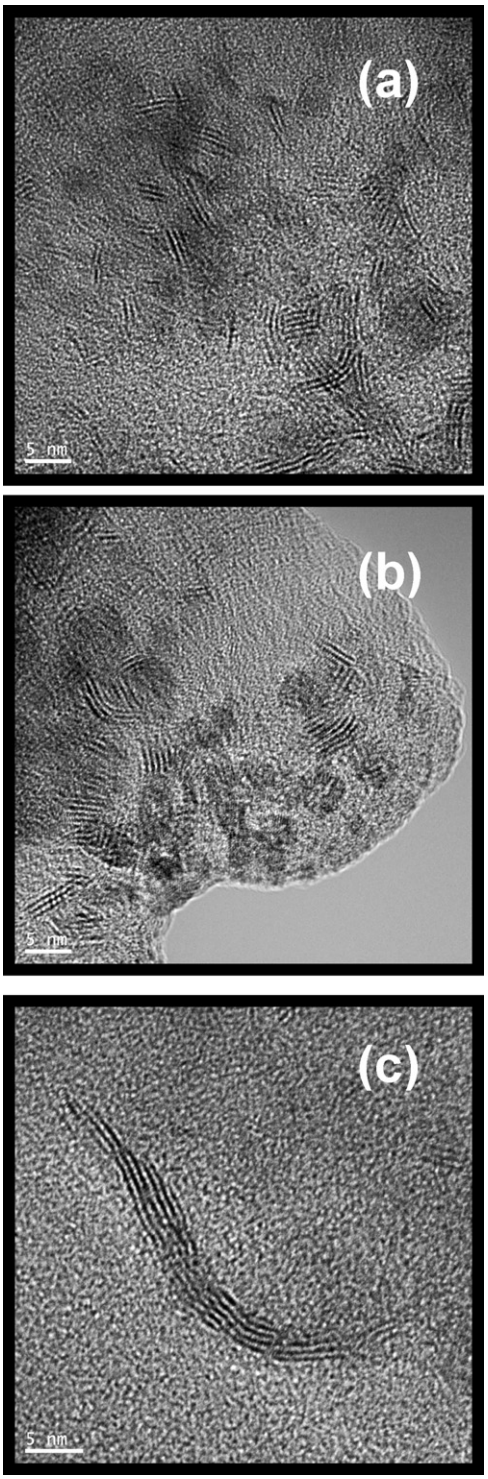

Fig. 9. High magnification TEM images of Mo(W)S_2 sheets observed on sulphided catalysts: (a) NiMoW/Al-HMS; (b) CoMoW/Al-HMS; and (c) CoMoW/Al-SBA16.

when the CoS_2 phase is detected, the "Co-Mo(W)-S" active phase is preferentially formed [58]. Considering the percentage of sulphided Co species given in parenthesis in Table 4, as determined from the area of the respective peaks, it appears that the degree of sulphidation of CoMoW/Al-HMS and CoMoW/Al-SBA16 samples is relatively low (61 and 57%, respectively). This is in good agreement with TPR study suggesting strong interactions between Mo(W) and Co on the surface of both Al-HMS and Al-SBA16 samples.

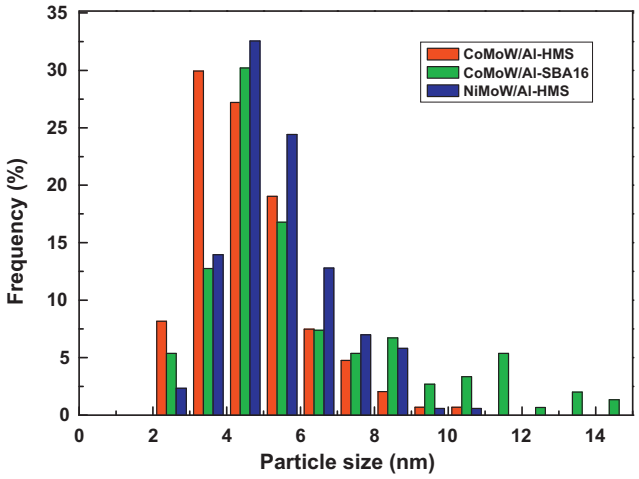

Fig. 10. Mo/(W)S_2 particle size distribution for the sulphided catalysts as determined by statistical analysis of HRTEM data.

Concerning the Mo 3*d* core level spectra (Fig. 12(a)), one doublet with the $3d_{5/2}$ and $3d_{3/2}$ components from the spin–orbit splitting suggests only the presence of one type of molybdenum species. In all cases, the Mo $3d_{5/2}$ component is located at 228.7–228.8 eV, close to that reported for the MoS_2 species (229.0 eV) [57]. As MoO_3 is sulphided at a faster rate than WO_3, tungsten species were partially sulphided in all catalysts. In order to estimate the fraction of sulphided W^{IV} species present in both series of catalysts, the W 4*f*

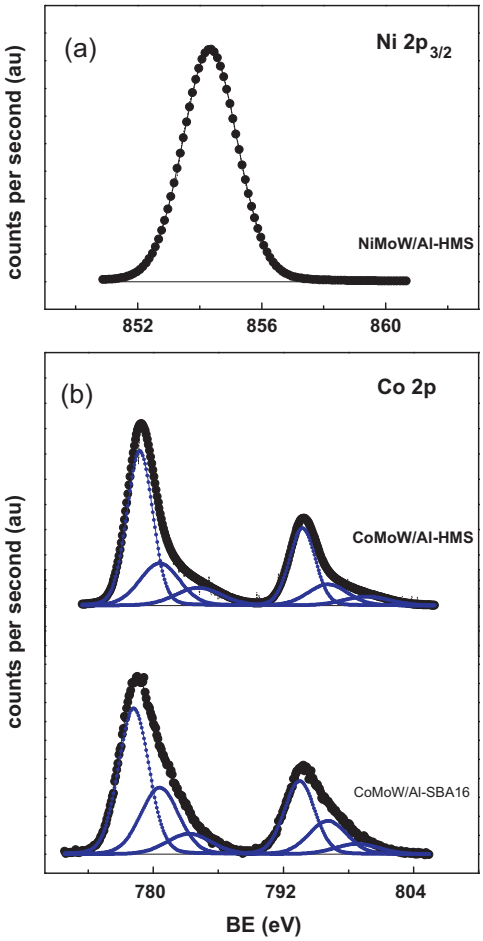

Fig. 11. Ni2p (a) and Co2p (b) core level spectra of sulphided catalysts.

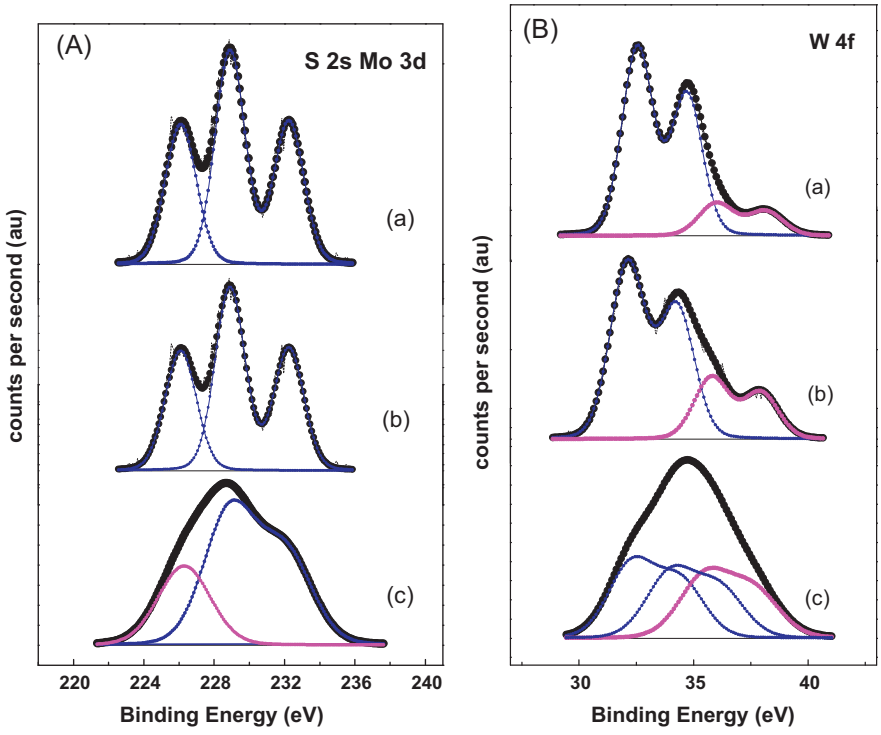

Fig. 12. S2s–Mo3d (A) and W4f (B) core-level spectra of sulphided catalysts: (a), NiMoW/Al-HMS; (b), CoMoW/Al-HMS; and (c), CoMoW/Al-SBA16.

signals were fitted assuming the coexistence of both sulphide and oxysulphide species. For all catalysts, the W $4f_{7/2}$ binding energy values ranging from 32.3 to 34.0 have been assigned to W^{4+} species in a WS_2-like structure [58,59]. An additional peak at 35.5–36.0 eV is consistent with the presence of an oxosulphide W(VI) species [58].

The influence of support morphology on the surface exposure of supported Co, Mo and W species was estimated by comparing the Co/Si, W/Si and Mo/Si atomic intensity ratios of both CoMoW/Al-HMS and CoMoW/Al-SBA16 catalysts (Table 5). In general, it was found that both Al-HMS-based catalysts recorded a larger surface exposure of their metal species than their CoMoW/Al-SBA16 counterpart, in good agreement with the normalized NS_{BET} (Table 1). Both Co-promoted catalysts record a similar degree of sulphidation, as deduced from the comparison of the S/[Co + Mo + W] atomic ratios (see last column in Table 5). In good agreement with TPR data (Fig. 8), the NiMoW/Al-HMS catalyst records a larger sulphidation degree than its two Co-promoted counterparts.

3.3. Catalyst activity

The catalytic performance of Ni- and Co-promoted MoW/Al-HMS and MoW/Al-SBA16 catalysts for the HDS of DBT was studied in a batch reactor at 350 °C under 3.1 MPa of total hydrogen pressure. DBT conversions at a reaction time of 5 h are compiled in Table 6 and DBT conversion versus reaction time is shown in Fig. 13(a). The overall activity of NiMoW/Al-HMS is superior to that of CoMoW/Al-HMS and CoMoW/Al-SBA-16 over the entire reaction time explored. At reaction time of 5 h, the Al-HMS-supported Ni-and Co-promoted samples have a DBT conversion of 60.5% and 50.6%, respectively. As compared with the CoMoW/Al-HMS, the CoMoW/Al-SBA16 has half the DBT conversion (26.8%). The plots of DBT conversion versus reaction time (Fig. 13(a)) point out to a pseudo-first order kinetics for all catalysts studied, which is in agreement with recently reported kinetics by Farag [33] for the HDS of DBT reaction performed in an autoclave over unsupported NiMo and CoMo sulfide catalysts. Fig. 13(b) shows the results of HDS catalytic activity expressed as the pseudo-first order kinetic constants of the catalysts. Results for laboratory-made catalysts are compared to a commercial $CoMo/Al_2O_3$ catalyst. An inspection of this figure reveals the following activity trend: NiMoW/Al-HMS > CoMoW/Al-HMS > $CoMo/Al_2O_3$ > CoMoW/Al-SBA16. This trend indicates that, under the reaction conditions used, Ni is more effective as a promoter than Co. The opposite results were observed for Ni- and Co-promoted Mo/Al-HMS catalysts tested in the HDS of thiophene performed in a flow reactor [23]. The reactivity of the CoMoW/Al-HMS catalyst is a little lower than that of the NiMoW/Al-HMS catalyst. The specific kinetic rate constants of all the catalysts studied were two orders of magnitude greater than those reported for CoMo/C [60] and bulk MoS_2 [61] catalysts tested under similar reaction conditions.

To elucidate the influence of support morphology and the effect of the promoter on the reaction pathways in the HDS of DBT, Table 6 summarises product distributions at the same DBT conversion (24%). For all the catalysts studied, the products detected were THDBT, CHB, BP and DCH. Hydrocracking products, such as benzene and cyclohexane, were not detected. According to the literature [62], the HDS of DBT over the catalysts studied occurs through two parallel reaction pathways (Scheme 1): (i) hydrogenation (HYD) of one and two aromatic rings of DBT leading to the formation of intermediate THDBT and CHB, respectively; and (ii) direct desulphurization (DDS) route, which involves the hydrogenolysis of C-S with no hydrogenation of the aromatic rings (BP formation). For both Co-promoted catalysts, the BP was the main product, indicating that the DDS route of DBT transformation is preferential for those catalysts. Contrary to those catalysts, the Ni-promoted catalyst records a large formation of CHB and DCH, indicating much larger hydrogenation properties of this sample with respect to both Co-promoted counterparts.

In order to obtain more precise information about the hydrogenation properties of catalysts, the HYD/DDS selectivity ratio was calculated for the same DBT conversion (24%). Fig. 13(c) compares

Table 6
DBT conversion and products distribution in HDS of DBT.

Catalyst	DBT[a] conv. (%)	Product distribution[b] (%)			
		THDBT	BP	CHB	DCH
NiMoW/Al-HMS	60.5	0.0	3.6	10.4	9.9
CoMoW/Al-HMS	50.6	1.2	12.6	3.6	5.1
CoMoW/Al-SBA16	26.8	2.2	14.5	3.3	3.6

[a] Reaction conditions were: $T = 350\,^{\circ}C$, $P_{H_2} = 3.1$ MPa, $t = 5$ h.
[b] Achieved at DBT conversion of 24%.
THDBT: tetrahydrodibenzothiophene; BP: biphenyl; CHB: cylohexylbenzene; DCH: dicylohexyl.

their HYD/DDS ratio with that of a commercial $CoMo/Al_2O_3$ catalyst. As seen, the HYD/DDS ratio follows the trend: NiMoW/Al-HMS > > CoMoW/Al-HMS > CoMoW/Al-SBA16 > $CoMo/Al_2O_3$. Thus, the CoMoW/Al-SBA16 catalyst, which has the lowest amount of Al-atoms incorporated into its support framework (from Al^{27} NMR), has a lower HYD activity than its CoMoW/Al-HMS counterpart. This is in good agreement with a study by Klimova et al. [28], who observed that when Al-atoms are incorporated into the SBA-16-support, the proportion of HYD route products decreases. The HYD/DDS ratio of the NiMoW/Al-HMS sample was found to be considerably higher than as reported for the binary NiMo/Al-HMS catalyst (5.64 vs. 0.18) [21] indicating that the ternary NiMoW/Al-HMS catalyst has much larger hydrogenation activity with respect to its binary NiMo/Al-HMS counterpart.

Finally, it is noteworthy that CoMoW/Al-HMS activity is close to that of a commercial $CoMo/Al_2O_3$ catalyst. Therefore, it appears that the Al-HMS substrate has special properties to give high activity in the supported metal sulphide phases. Similarly, a comparison of the HDS activity of WS_2/Al-HMS [23] and MoS_2/Al-HMS [22] catalysts with a γ-Al_2O_3-supported one indicates that Al-HMS-based catalysts record outstanding activity.

3.4. Catalyst activity-structure correlation

3.4.1. Influence of support

In order to assess the support effect (Al-HMS vs. Al-SBA16) on catalytic functionalities and understand how these catalysts perform in comparison with an industrial $CoMo/Al_2O_3$ catalyst, a comparative study of CoMoW/Al-HMS and CoMoW/Al-SBA16 catalysts is made. This comparison, shown in Fig. 13(a) and (b), indicates that an Al-HMS-supported catalyst is more active than its Al-SBA16-supported counterpart. This is surprising, as one might expect that the 3D structure of the Al-SBA-16 material might provide more favourable mass transfer kinetics than the 2D hexagonal arrangement of pore system of the Al-HMS substrate. The lowest activity of the CoMoW/Al-SBA16 catalyst among the catalysts studied is likely due to the fact that it records partial blocking of the pores by the guest molecules, as deduced by the normalized BET specific surface area of the oxide catalyst precursors (Table 1), which helps to decrease the accessibility of the DBT molecules to the active sites. Moreover, a comparison of the average pore diameter of the two CoMoW/Al-HMS and CoMoW/Al-SBA16 catalysts (Table 1) suggests that the higher activity of the former should be linked to its larger pore size (5.0 vs. 1.7 nm), favouring the diffusion of a large DBT molecule into the inner porous structure of this catalyst. Thus, the mesopores of the Al-HMS substrate are particularly suited for processing heavy oil feeds. The possible influence of the specific surface area could be excluded because all the catalysts have a similar S_{BET} (Table 1).

In this work, a strong influence of the support type on the phases formed is observed by XRD (Fig. 5) and HRTEM (Fig. 9(b) and (c)). On the one hand, the formation of large crystals of β-$CoMo(W)O_4$ on the CoMoW/Al-HMS oxide precursor (from XRD) suggests a low metal-support interaction. Considering that loosely bound phases are highly reducible and easily sulphided, they provide a relatively high concentration of S-vacancies in CoMoW/Al-HMS catalyst [63]. Indeed, as the surface exposure of the metal sulphide species of CoMoW/Al-HMS was twice that of CoMoW/Al-SBA16 (see XPS data in Table 5), the former catalyst is expected to be more active. After sulphidation, the more active CoMoW/Al-HMS has a mixture of short and long $Mo(W)S_2$ slabs randomly oriented on the Al-HMS support (Fig. 9(b)), whereas its CoMoW/Al-SBA-16 counterpart has so-called "onion-type" $Mo(W)S_2$ structures (Fig. 9(c)). Assuming the basal plane of the $Mo(W)S_2$ phase is not catalytically active, whereas the Mo(W)-atoms at edge and corner locations play an important role in HDS activity [64], the lowest activity of the CoMoW/Al-SBA16 catalyst could be explained in terms of the formation of "onion-type" $Mo(W)S_2$ crystalline phases with a large number of basal planes (Fig. 9(c)). In this sense, it is hypothesised that the presence of extraframework $AlNO_3$ phases on the surface of CoMoW/Al-SBA16 favours the formation of a less

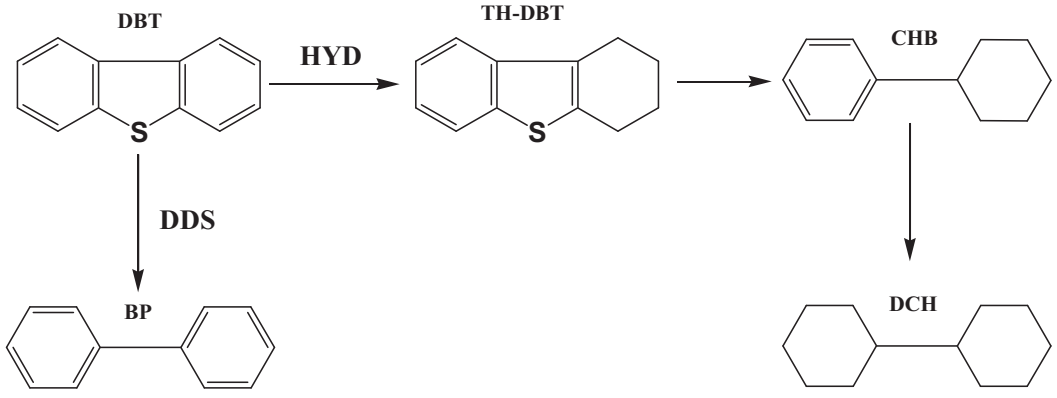

Scheme 1. Reaction scheme for the HDS of DBT over Ni(Co)MoW sulphided catalysts supported on Al-HMS and Al-SBA16 substrates: direct desulphurization (DDS), hydrogenation (HYD), dibenzothiophene (DBT), tetrahydrodibenzothiophene (TH-DBT), biphenyl (BP), cyclohexylbenzene (CHB), dicyclohexyl (DCH).

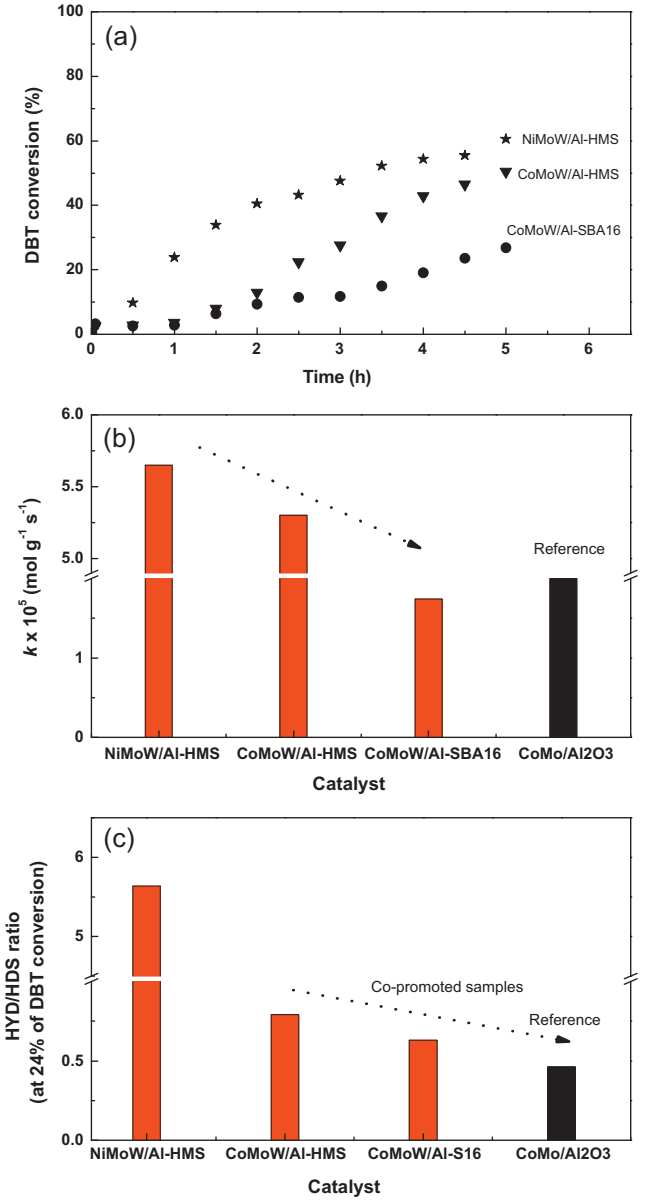

Fig. 13. DBT conversion versus reaction time (a), pseudo-first order kinetic constants (b) and HYD/DDS selectivities ratio (c) in the HDS of DBT ($T = 350\,^{\circ}C$; P_{H_2} = 3.1 MPa; batch reactor) on supported Ni(Co)MoW and a commercial $CoMo/Al_2O_3$ catalysts.

active "onion-type" $Mo(W)S_2$ structure. The negative effect of the formation of "onion-type" crystalline phases on HDS activity was observed also for Ni-MoS_2/SBA-15 HDS catalysts [65].

3.4.2. Influence of promoter (Ni vs. Co)

The Ni-promoted MoW/Al-HMS catalyst present a larger HDS activity than its Co-promoted MoW/Al-HMS counterpart, in good agreement with the study on binary Ni(Co)-Mo(W) catalysts supported on MCM-41 doped with zirconium [66]. Similarly, a predictive approach, using density functional theory (DFT) calculation and experiments performed with Co and Ni promoted ternary systems tested in the HDS of thiophene and of straight run gas oil, confirmed that the $NiMo_{0.5}W0.5/Al_2O_3$ catalyst was more active (about 30%) than reference $NiMo/Al_2O_3$ catalyst containing equivalent atoms loadings, whereas its Co-promoted counterpart did not reveal any synergy effects [67].

A general observation regarding the HDS of DBT over NiMoW/Al-HMS catalyst is that hydrogenation prevails over hydrogenolysis

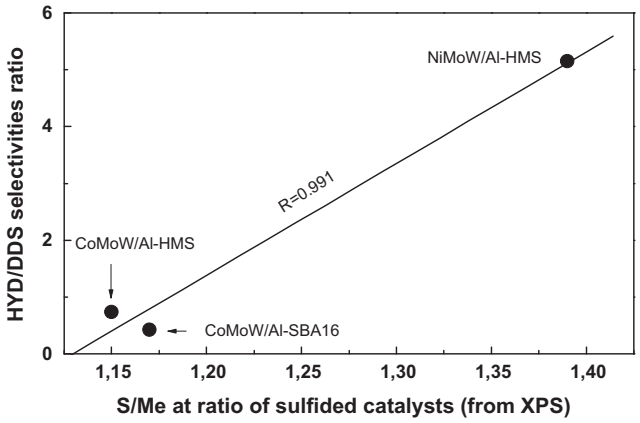

Fig. 14. Correlation between HYD/DDS selectivity's ratio (achieved at DBT conversion of 24%) and sulphidation degree of the catalysts, as determined from S/Me atomic ratio (XPS).

(Scheme 1), whereas direct desulphurization prevails over hydrogenation for both Co-promoted catalysts (Fig. 13(c)), as was already observed in unsupported ternary CoMoW catalysts [30]. The outstanding hydrogenation behaviour of the nickel-promoted catalyst is probably due to the widely reported larger intrinsic hydrogenation activity of Ni with respect to Co. However, a linear correlation between the HYD/DDS selectivity ratio and the degree of sulphidation of species (Fig. 14) strongly suggests that the enhancement of hydrogenation over Ni-promoted catalyst could be linked with a larger proportion of sulphided phases with respect to its Co-promoted counterpart. Indeed, the Ni-promoted catalyst has the largest surface density of $Mo(W)S_2$ particles among the catalysts studied, as deduced from HRTEM (Table 3). Interestingly, the NiMoW/Al-HMS catalyst has a hydrogenation activity (HYD/DDS = 5.64) that is ten-times greater than a commercial $NiMo/Al_2O_3$ catalyst (HYD/DDS = 0.53) tested by Huang et al. [65] under similar reaction conditions.

Considering the catalyst activity-structure correlation, the greater catalytic activity of the Ni-promoted catalyst as compared to the Co-promoted one could be explained in terms of the following factors: (i) the widely reported higher intrinsic hydrogenation properties of Ni as compared to cobalt [68], confirmed by the highest HYD/DDS selectivity ratio of the Ni-promoted catalyst among the catalysts studied (Fig. 13(c)); (ii) the lower amount of extra-framework Al-species, as deduced from ^{27}Al NMR measurements (Fig. 4); (iii) the lower metal-support interaction shown by TPR (Fig. 8), which leads to the easier reduction/sulphidation of the precursor metal oxide phases; (iv) the larger degree of sulphidation of exposed surface species on the support surface, as derived from XPS (Table 5); and (v) the higher acidity, as deduced from TPD-NH_3 of the oxide precursors (Table 2). By comparing all the above factors, the influence of the surface exposure of metal sulphide species on catalyst activity was of minor importance (Table 5). By contrast, the lower activity of the CoMoW/Al-HMS with respect to NiMoW/Al-HMS may be related to the larger amount of $Mo^{6+}(W^{6+})$ ions in tetrahedral coordination, as determined by DRS UV–vis (Fig. 6). Tetrahedral species are difficult to reduce or sulphide, and cannot therefore develop HDS active sites. Indeed, the direct correlation between the reducibility of the oxidic precursors and the HDS activity of the sulphided samples is widely reported in the literature [69,70].

4. Conclusions

A new class of potential Al-HMS and Al-SBA-16 supports for ternary Ni(Co)MoW HDS catalysts has been prepared by the

one-pot sol–gel synthesis method via the neutral templating pathway using dodecylamine and Pluronic F127 as surfactants, respectively. From the HDS of DBT reaction results, the main conclusions of this study are as follows: (i) Ni is more effective as a promoter than Co; (ii) the Al-HMS substrate is more effective than its Al-SBA-16 counterpart due to its much larger pore size (5.0 vs. 1.8 nm), favouring the diffusion of the DBT molecules in the inner pore network of this catalyst; (iii) the presence of extraframework $AlNO_3$ phases on the surface of CoMoW/Al-SBA16 might compromise its HDS activity because of the formation of a less active "onion-type" $Mo(W)S_2$ structure; and (iv) under the reaction conditions used, the NiMoW/Al-HMS catalyst was found to be more active than a commercial $CoMo/Al_2O_3$ catalyst. This is an important finding of this research because it offers the possibility of preparing highly effective HDS catalysts.

Acknowledgement

This work was supported by CONACYT, PROMEP PTC 273 and CIC-UMSNH programmes (Mexico), with financial aid from the Scientific Cooperation FONCICYT Programme (FONCICYT-96194 project), the Spanish Ministry of Science and Innovation (ENE2010-15387-C02-01) and the Community of Madrid (S2009ENE-1743 project).

References

[1] H. Topsøe, B.S. Clausen, F.E. Massoth, in: J.R. Anderson, M. Boudart (Eds.), Hydrotreating Catalysis. Science and Technology, vol. 11, Springer-Verlang, Berlin Heidelberg, 1996.
[2] B. Pawelec, R.M. Navarro, J.M. Campos-Martin, J.L.G. Fierro, Catalysis Science & Technology 1 (2011) 23–42.
[3] F.L. Plantenga, R.G. Leliveld, Applied Catalysis A-General 248 (2003) 1–7.
[4] S.L. Soled, S. Miseo, R. Krikak, H. Vroman, T.H. Ho, K.L. Riley, US Patent 6, 299, 760 B1 (2001).
[5] M. Alibouri, S.M. Ghoreishi, H.R. Aghabozorg, Journal of Supercritical Fluids 49 (2009) 239–248.
[6] M. Alibouri, S.M. Ghoreishi, H.R. Aghabozorg, Industrial & Engineering Chemistry Research 48 (2009) 4283–4292.
[7] R. Huirache-Acuña, B. Pawelec, E. Rivera-Muñoz, R. Nava, J. Espino, J.L.G. Fierro, Applied Catalysis B: Environmental 92 (1–2) (2009) 168–184.
[8] C.F. Cheng, Y.C. Lin, H.H. Cheng, Y.C. Chen, Chemical Physics Letters 382 (2003) 496–501.
[9] W.J.J. Stevens, K. Lebeau, M. Mertens, G. Van Tendeloo, P. Cool, E.F. Vansant, Journal of Physical Chemistry B 110 (2006) 9183–9187.
[10] J.M.R. Gallo, C. Bisio, L. Marchese, H.O. Pastore, Microporous Mesoporous Materials 111 (2008) 632–635.
[11] B. Pawelec, S. Damyanova, R. Mariscal, J.L.G. Fierro, I. Sobrados, J. Sanz, L. Petrov, Journal of Catalysis 223 (2004) 86–97.
[12] A. Sayari, Chemistry of Materials 8 (1996) 1840–1852.
[13] K.-Ch. Park, D.-J. Yim, S.-Ki Ihm, Catalysis Today 74 (2002) 281–290.
[14] R. Schmidt, D. Akporiayea, M. Stöcker, O.H. Ellestad, Studies in Surface Science and Catalysis 84 (1994) 61–68.
[15] R. Ryoo, M.J. Kim, Chemical Communications 22 (1997), 2255-2226.
[16] M.L. Occelli, S. Biz, A. Auroux, G.J. Ray, Microporous Mesoporous Materials 26 (1998) 193–213.
[17] R. Mokaya, Journal of Catalysis 186 (1999) 470–477.
[18] D. Trong On, D. Desplantier-Giscard, C. Danumah, S. Kaliaguine, Applied Catalysis A-General 253 (2003) 545–602.
[19] Y. Sun, R. Prins, Angewandte Chemie International Edition 47 (2008) 8478–8481.
[20] A.M. Venezia, R. Murania, V. La Parola, B. Pawelec, J.L.G. Fierro, Applied Catalysis A-General 383 (2010) 211–216.
[21] T.A. Zepeda, B. Pawelec, J.L.G. Fierro, A. Olivas, S. Fuentes, T. Halachev, Microporous Mesoporous Materials 111 (2008) 157–170.
[22] T. Chiranjeevi, P. Kumar, M.S. Rana, G. Murali Dhar, T.S.R. Prasada Rao, Journal of Molecular Catalysis A: Chemical 181 (2002) 109–117.
[23] T. Chiranjeevi, P. Kumar, M.S. Rana, S.K. Maity, G. Murali Dhar, T.S.R. Prasada Rao, Microporous Mesoporous Materials 44–45 (2001) 547–556.
[24] T. Halachev, J.A. De los Reyes, C. Araujo, L. Dimitrov, G. Córdoba, L. Dimitrov, Studies in Surface Science and Catalysis 127 (1999) 401–404.
[25] M. Alibouri, S.M. Ghoreishi, H.R. Aghabozorg, Chemical Engineering Transactions 17 (2009) 1005–1010.
[26] T. Klimova, J. Reyes, O. Gutiérez, L. Lizama, Applied Catalysis A-General 335 (2008) 159–171.
[27] M. Gómez-Cazalilla, A. Infantes-Molina, R. Moreno-Tost, P.J. Maireles-Torres, J. Mérida-Robles, E. Rodríguez-Castellón, A. Jiménez-López, Catalysis Today 143 (2009) 137–144.
[28] T. Klimova, L. Lizama, J.C. Amezcua, E. Torrés, J. Navarrete, J.M. Domínguez, Catalysis Today 98 (2004) 141–150.
[29] T.R. Pauly, Y. Liu, T.J. Pinnavaia, S.J.L. Billinge, T.P. Rieker, Journal of the American Chemical Society 121 (1999) 8835–8842.
[30] R. Huirache-Acuña, M.A. Albiter, C. Ornelas, F. Paraguay-Delgado, R. Martínez-Sánchez, G. Alonso-Nuñez, Applied Catalysis A-General 308 (2006) 134–142.
[31] W. Zhang, T.R. Pauly, T.J. Pinnavaia, Chemistry of Materials 9 (1997) 2491–2498.
[32] K. Flodström, V. Alfredsson, Microporous Mesoporous Materials 59 (2003) 167–176.
[33] H. Farag, Journal of Colloid and Interface Science 348 (2010) 219–226.
[34] P.T. Tannev, M. Chibwe, T.J. Pinnavaia, Nature 368 (1994) 321–323.
[35] A.Y. Khodakov, A. Griboval-Constant, R. Bechara, F.J. Villain, Journal of Physical Chemistry B 105 (2001) 9805–9811.
[36] J.A. Hernandez, S. Gómez, B. Pawelec, T.A. Zepeda, Applied Catalysis B: Environmental 89 (2009) 128–136.
[37] S.J. Gregg, K.S.W. Sing (Eds.), Adsorption, Surface Area and Porosity, Academic Press, London, 1982.
[38] J.P. Gilson, G.C. Edwards, A.W. Peters, K. Rajagopalan, R.F. Wormsbecher, T.G. Roberie, M.P. Shatlocks, Journal of the Chemical Society, Chemical Communications (1987) 91–92.
[39] A. Yin, X. Guo, W.-L. Dai, K. Fan, Journal of Physical Chemistry C 114 (2010) 8523–8532.
[40] T. Chiranjeevi, G. Muthu Kumaran, J.K. Gupta, G. Murali Dhar, Thermochimica Acta 443 (2006) 87–92.
[41] A. Tuel, S. Gontier, Chemistry of Materials 8 (1996) 114–122.
[42] J.J. Fitzgerald, S.D. Kohl, G. Piedra, Chemistry of Materials 6 (1994) 1915–1917.
[43] R. Nava, R.A. Ortega, G. Alonso, C. Ornelas, B. Pawelec, J.L.G. Fierro, Catalysis Today 127 (2007) 70–84.
[44] K. Bourikas, C. Kordulis, A. Lycourghiotis, Catalysis Reviews – Science and Engineering 48 (2006) 363–444.
[45] J. Vakros, K. Bourikas, C. Kordulis, A. Lycourghiotis, Journal of Physical Chemistry B 107 (2003) 1804–1813.
[46] J.G. Graselli, B.J. Bulkin, Analytical Raman Spectroscopy, Wiley, New Cork, 1991, p. 352.
[47] Z. Zhang, J. Suo, X. Zhang, S. Li, Applied Catalysis A: General 179 (1999) 11–19.
[48] R.A. Schoonheydt, Diffuse reflectance spectroscopy, in: F. Delannay (Ed.), Characterization of Heterogeneous Catalysts, Marcel Dekker, New York, 1984, p. 125.
[49] D.K. Lee, H.T. Lee, I.Ch. Lee, S.K. Park, S.Y. Bae, Ch.H. Kim, S.I. Woo, Journal of Catalysis 159 (1996) 219–229.
[50] P. Gajardo, P. Grange, B. Delmon, Journal of Physical Chemistry 83 (1979) 1771–1779.
[51] J.E. Herrera, D.E. Resasco, Journal of Catalysis 221 (2004) 354–364.
[52] H.K. Matralis, Ch. Papadopoulou, A. Lycourghiotis, Applied Catalysis A: General 116 (1994) 221–236.
[53] S.K. Park, V. Kurshev, C.W. Lee, L. Kevan, Applied Magnetic Resonance 19 (2000) 21–33.
[54] Ch. Papadopoulou, J. Vakros, H.K. Matralis, G.A. Voyiatzis, Ch. Kordulis, Journal of Colloid and Interface Science 274 (2004) 159–166.
[55] R. Nava, J. Morales, G. Alonso, C. Ornelas, B. Pawelec, J.L.G. Fierro, Applied Catalysis A: General 321 (2007) 58–70.
[56] K.T. Ng, D.M. Hercules, Journal of Physical Chemistry 80 (1976) 2094–2102.
[57] C.D. Wagner, in: D. Briggs, M.P. Seah (Eds.), Practical Surface Analysis by Auger and X-ray Photoelectron Spectroscopy, John Willey, Chichester, 1983.
[58] Z. Le, P. Afanasiev, D. Li, X. Long, M. Vrinat, Catalysis Today 130 (2008) 24–31.
[59] J.N. Fiedor, A. Proctor, M. Houalla, D.M. Hercules, Surface and Interface Analysis 23 (1995) 204–212.
[60] H. Farag, D.D. Whitehurst, K. Sakanishi, I. Mochida, Catalysis Today 50 (1999) 49–56.
[61] H. Farag, K. Sakanishi, M. Kouzu, A. Matsumura, Y. Sugimoto, I. Saito, Catalysis Communications 4 (2003) 321–326.
[62] P.T. Vasudevan, J.L.G. Fierro, Catalysis Reviews – Science and Engineering 38 (1996) 161–188.
[63] J. Vakros, C. Kordulis, Applied Catalysis A: General 217 (2001) 287–293.
[64] M. Daage, R.R. Chianelli, Journal of Catalysis 149 (1994) 414–427.
[65] Z.D. Huang, W. Bensch, L. Kienle, S. Fuentes, G. Alonso, C. Ornelas, Catalysis Letters 127 (2009) 132–142.
[66] E. Rodríguez-Castellón, A. Jiménez-López, D. Eliche-Quesada, Fuel 87 (2008) 1195–1206.
[67] C. Thomazeau, C. Geantet, M. Lacroix, M. Danot, V. Harlé, P. Raybaud, Applied Catalysis A: General 322 (2007) 92–97.
[68] M. Vrinat, M. Lacroix, M. Breysse, L. Mosoni, M. Roubin, Catalysis Letters 3 (1989) 405–412.
[69] F.E. Massoth, Journal of Catalysis 36 (1975) 164–184.
[70] V.H.J. De Beer, C. Bevelander, T.H.M. van Sint Fiet, P.G.A. Werter, C.H. Amberg, Journal of Catalysis 43 (1976) 68–77.